PCCP

Accepted Manuscript

ROYAL SOCIETY OF CHEMISTRY

www.rsc.org/pccp

Physical Chemistry Chemical Physics
CREATED USING THE RSC LaTeX PCCP ARTICLE TEMPLATE – SEE www.rsc.org/electronicfiles FOR DETAILS
ARTICLE TYPE www. rsc.org/x XXXXXXXX

Flatbands in 2D boroxine-linked covalent organic frameworks

Rui-Ning Wang, Xin-Ran Zhang, Shu-Fang Wang,* Guang-Sheng Fu, and Jiang-Long Wang‡

Received Xth September 2015, Accepted Xth XXXXXXXXX 2015
First published on the web Xth XXXXXXXXXX 2015
DOI: 10.1039/b000000x

Density functional calculations have been performed to analyze the electronic and mechanical properties of a number of 2D boroxine-linked covalent organic frameworks (COFs), which are experimentally fabricated by the di-borate aromatic molecules. Further, the band structures are surprising and show the flat-band characteristics which are mainly attributed to the delocalized $\pi-$conjugated electrons around the phenyl rings and can be better understood within the aromatical theory. Next, the effects of branch sizes and hydrostatic strains on their band structures are systematically considered within generalized gradient approximations. It is found that their band gaps will start to saturate when the branch size reaches 9. For boroxine-linked COFs with only one benzene ring in the branch, the band gap is robust under the compressive strain while it decreases with the tensile strain increasing. When the branch size is equal or greater than 2, their band gaps will monotonously increase with the strain increasing in the range of [-1.0, 2.0] Å. All boroxine-linked COFs are semiconductors with the controllable band gaps, depending on the branch length and the applied strain. In comparison with other 2D materials, such as graphene, hexagonal boron nitride, and even γ-graphyne, all boroxine-linked COFs are much softer and even more stable. That is, they can maintain the planar features under a larger compressive strain, which means that they are good candidates in the flexible electronics.

1 Introduction

Recently, 2D ultrathin materials have been experimentally synthesized and characterized, such as the archetypical graphene,[1] hexagonal boron nitride,[2] transition metal dichalcogenides,[3] silicene,[4] germanene,[5] phosphorene,[6] and even hafnium honeycomb layers.[7] They usually have atomically thin and robust structures and unique electronic properties, so they have generated immense interests for many emerging fields.[8,9] Generally, all of them belong to inorganic nanomaterials. By comparison, covalent organic frameworks (COFs), composed entirely of light chemical elements and originally shown in 2005, are with tunable structural motifs but low intrinsic conductivity.[10–12] Structurally similar to graphene, they are constructed in place of carbon atoms with small organic molecules.[13,14] Furthermore, because of their π-stacked columns which can drive the electronic interactions between the nearest neighbor sheets and furtherly provide a path for charge carriers migration,[15] they are the promising molecular semiconductors in the photovoltaic device.[16,17]

However, the mechanical exfoliation of bulk COFs to a monolayer is practically very difficult due to the limited sizes of COFs. Therefore, 2D COFs are experimentally fabricated *via* the bottom-up preparative technique. For instance, well-ordered 2D boronic acid based COFs can be fabricated by the dehydration of di-borate aromatic molecules.[18,19] This is because that the chemical equilibrium could be kept by adding a small amount of water into the closed reaction system. Further, boronic acid based COFs are of special interest due to their ability to form lamellar eutectic structures.[20,21] As is well known, the electronic properties of 2D COFs could be predictably tuned by controlling a few of degrees of freedom,[22] such as the branch chains, radical cations, morphologies, and dopants. For example, when the dopants such as I_2 and tetracyanoquinodimethane diffusive into the tetrathiafulvalene-based COFs, the redox reactions happen which facilitate the cross-layer delocalization of tetrathiafulvalene radical cations to generate higher conductivity as high as 0.28 S m^{-1}.[23]

In this study, nine different kinds of boroxine-linked COFs with various lengths of phenyl rings, namely benzene-n (n=1∼9), are taken into consideration. And then, we have systematically calculated their band structures. In the vicinity of the Fermi level, the bands are very flat and show narrow-band characteristics. From the analysis of the frontier molecular orbital distribution and aromaticity theory, this is mainly because of the delocalized π-conjugated electrons around the phenyl rings. Strains are often applied to tune the electronic properties of graphene-like sheets.[24,25] Moreover, Meunier et al. studied the effect of the hydrostatic strain on the electronic properties of benzene-1, but the investigations on other boroxine-linked COFs are lacked.[22] Therefore, *ab-initio* strain energy calculations within the harmonic elastic deforma-

Hebei Key Lab of Optic-Electronic Information and Materials, College of Physics Science and Technology, Hebei University, Baoding 071002, P. R. China
* E-mail:swang2008@hotmail.com
‡ E-mail:jlwang@hbu.edu.cn

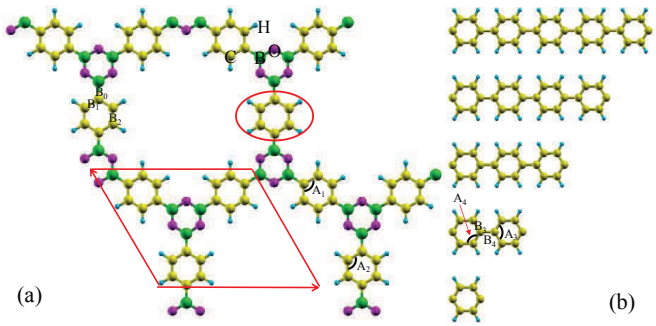

Fig. 1 (Color online). Atomic configurations of 2D boroxine-linked COFs (a). The parallelogram shows the unit cell. The ovals mean that various benzene rings can be connected between two boroxine rings (b). The lengths (n) of benzene rings increase from n=1 to 5. For all the atomic structures discussed in this paper, boron is shown in green, oxygen in orange, carbon in yellow, and hydrogen in blue.

tion range are applied to benzene-n with n=1∼5 and the strain-induced electronic structure changes and the Young's modulus are given. The results show that all these boroxine-linked COFs are semiconductors with the controllable band gaps, depending on the rational chemical design and the applied strain. Furthermore, their band gaps increase monotonously and steadily with the strain in the range of [-1.0, 2.0] Å, while for benzene-1, an asymmetry tunable band gap occurs. The tensile strain makes the band gap decrease from 3.55 to 3.00 eV while the band gap is robust under the compressive strain.

The paper is organized as follows. In Sec. II, the computational details are briefly introduced. In Sec. III, we present our self-consistently calculated flat bands, Young's modulus, and the changes of the band gaps. The paper ends with Sec. IV where a short conclusion is given.

2 CALCULATIONAL Details

The electronic properties of the systems shown in Fig. 1 are characterized *via ab-initio* calculations in the framework of density functional theory,[26] as implemented in the SIESTA package.[27] The generalized gradient approximation is applied for the exchange-correlation potential by using the Perdew-Burke-Ernzerhof functional.[28] A linear combination of a standard double zeta basis plus the polarization for describing all valence electrons and norm-conserving pseudopotentials[29] for the atomic core are employed. Integration inside of the first Brillouin zone is sampled on 10 × 10 × 1 Monkhorst-Pack meshgrids.[30] The real-space grid cutoff energy is 300 Ry and a Fermi-Dirac distribution function with an electronic temperature of 20 meV is used to populate the energy levels. The appropriate vacuum region (20 Å) is chosen in the direction normal to the surface which is much larger than the interlayer spacing of graphite (3.35 Å),[31] so each sheet can be laterally isolated from its periodic images.

3 RESULTS AND DISCUSSIONS

The atomic structures of 2D boroxine-linked COFs are shown in Fig. 1 (a). They are ideally honeycomb-like structures with six boroxine rings locating at the vertices of the hexagonal cell and show the $P6_3/mmc$ symmetry.[10] Six sides are composed of a series of benzene rings (Fig. 1(b)) which bring out the best in 2D boroxine-linked COFs: the pore size and electronic properties can be tuned by changing the benzene ring "bridges". Here, a series of 2D boroxine-linked COFs are taken into consideration and named after benzene-n according to the number (n) of benzene rings connected between two boroxine rings. Firstly, the equilibrium lattice constants (a_n) are obtained by a least-squares fit *via* the total energies ($E[a_n]$) after every geometry is fully optimized as a function of the lattice constants. The equilibrium lattice constants, as shown in Table I, are 15.11, 22.66, 30.26, 37.84, and 45.42 Å for n=1, 2, 3, 4, and 5, respectively. For benzene-1, the lattice constant is consistent with the previously calculated result (15.173 Å)[22] but slightly less than the experimental value (15.420 Å).[10] In general, our results are consistent with the experimentally measured pore sizes.[32] Table I also shows the concrete geometry parameters in detail. In all 2D boroxine-linked COFs, the boroxine ring is slightly different from the benzene ring. On one hand, the O-B bonds (1.38 Å) are less than C-C bonds (1.41 Å) in the benzene ring as those inside of graphene. On the other hand, the boroxine ring is not a perfect hexagon and the angle (∠BOB) is about 121° which is consistent with the previous results.[33] This is because that the electronegativity of oxygen elements is stronger and there are a lone pair of electrons mostly localized around oxygen atoms. Consequently, in comparison with benzene rings, the boroxine rings have very little aromatic characters.[34,35] For benzene-1 and benzene-2 boroxine-linked COFs, the boroxine and benzene rings are in a plane (see Supporting Information Figs. S1 and S4). Furthermore, when all the benzene rings are in a plane, benzene-n (n ≥ 3) boroxine-linked COFs are metastable (see Supporting Information Fig. S6). In addition, the torsion of the phenylene groups is very complex, especially for boroxine-linked COFs with an even number of benzene rings connected between the boroxine rings. This is because the dihedral angle between the phenylene groups is ∼39° (see Supporting Information Table SI). Therefore, only the planar geometries are taken into consideration in this study.

Once the equilibrium structures are determined, it is ready to investigate the ground-state properties of 2D boroxine-linked COFs. For benzene-1, the band structure and density of states are calculated and shown in Fig. 2. In the (a) panel, the band structure is plotted along a high symmetry k-direction, Γ-K-M-Γ, in the first Brillouin zone. Although it has a simi-

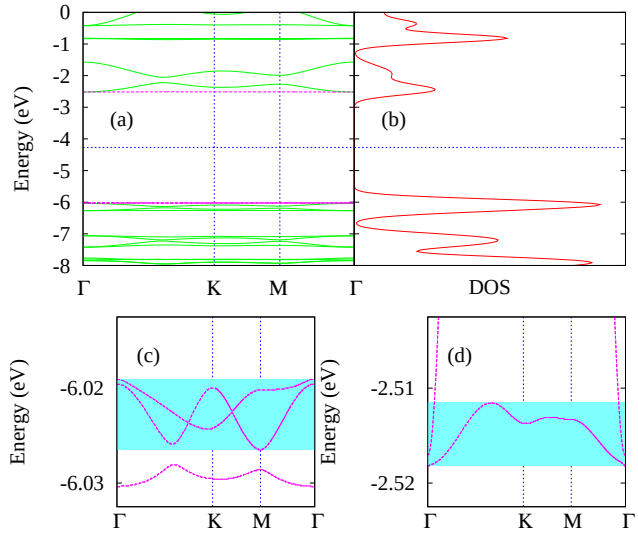

Fig. 2 (Color online). The calculated band structure (a) and density of states (b) of 2D boroxine-linked COF with only one benzene ring connected between two boroxine rings under zero strain. The enlarged views of HOMO (c) and LUMO (d) are also shown. The Fermi level is set at the middle of the valence and conduction bands.

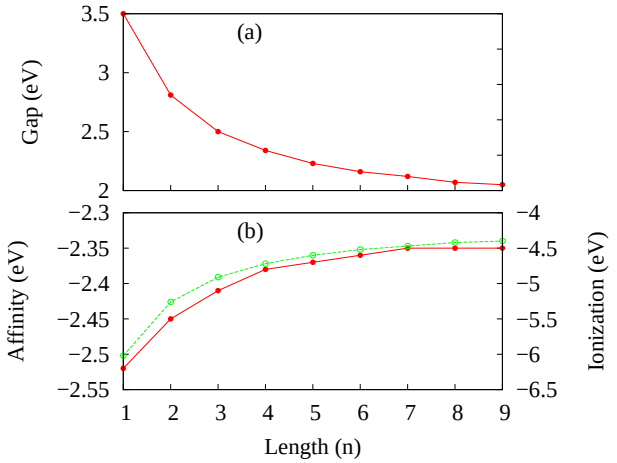

Fig. 3 (Color online). The energies (eV) of band gaps (a), electronic affinity (b) and ionization potential (b) of 2D boroxine-linked COFs as a function of the benzene lengths (n). The solid line (filled dots) and the dotted line (circles) refer to the electronic affinity and ionization potential, respectively.

lar topological structure to graphene, the electronic properties are completely different.[36] The latter presents a Dirac cone, while the former shows some flatbands over the whole Brillouin zone. Inspection of the density of states (Fig. 2(b)) reveals that 2D boroxine-linked COF with a benzene ring attains a band gap of $\sim$ 3.50 eV, which is consistent with the previously calculated value (3.55 eV).[22] In the vicinity of the Fermi level, the valence and conduction bands can not well disperse over the whole Brillouin zone, so the enlarged views of frontier orbital energies are redrawn to clearly distinguish the dispersion relation and shown in Figs. 2(c,d). It is found that the top of valence bands and the bottom of conduction bands are at the same position of Γ. The band widths for the highest occupied molecular orbitals (HOMO) and lowest unoccupied molecular orbitals (LUMO) are just only $\sim$ 7.4 meV and $\sim$ 6.7 meV, respectively. Moreover, the torsion of the phenyl ring around C-B bonds does not change the bandwidths of frontier orbitals except for the band gap (see Supporting Information Fig. S3). Generally, 2D benzene-1 boroxine-linked COF exhibits the direct band-gap semiconductor.

As the above-mentioned material design, a set of related structures are constructed by adding extra phenyl rings into the hexagonal sides. As shown in Fig. 3(a), all 2D boroxine-linked COFs exhibit the semiconducting characteristics and the band gaps will decrease with increasing the branch size (n). For example, the band gap reduces to 2.05 eV when the phenyl rings reach 9. According to our calculated results, the band gap of benzene-9 is mostly saturated. Using the vacuum-potential as the unique reference point, the reduction of their band gaps mainly owes to the increase of the ionization potential (or the valance-band maximum), although the electronic affinity (or the conduction-band minimum) also increases. From the panel (b) of Fig. 3, when n increases from 1 to 9, the ionization potential increases from -6.02 to -4.40 eV and the electronic affinity only increases from -2.52 to -2.35 eV. That is, the increase of ionization potential (1.62 eV) is ten times than that of electronic affinity (0.17 eV). In the following, the reason will be discussed by analyzing the local density of states. With increasing the benzene length, there is another difference in the frontier orbitals, as shown in Fig. 4. The first and second HOMO do not hybridize together but split apart from each other because a benzene ring is connected between the boroxine ring and another benzene ring which further breaks the hexagonal symmetry, as shown in Fig. 11. By contrast, the band widths of HOMO increase while they decrease for LUMO. Finally, the LUMO becomes a fully flat band over the whole Brillouin zone.

In order to elucidate the intrinsic characteristics of electron-

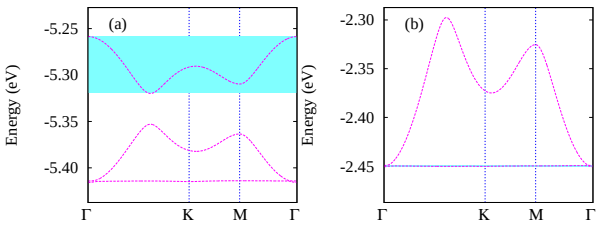

Fig. 4 (Color online). The enlarged views of HOMO (a) and LUMO (b) of benzene-2 boroxine-linked COF under zero strain.

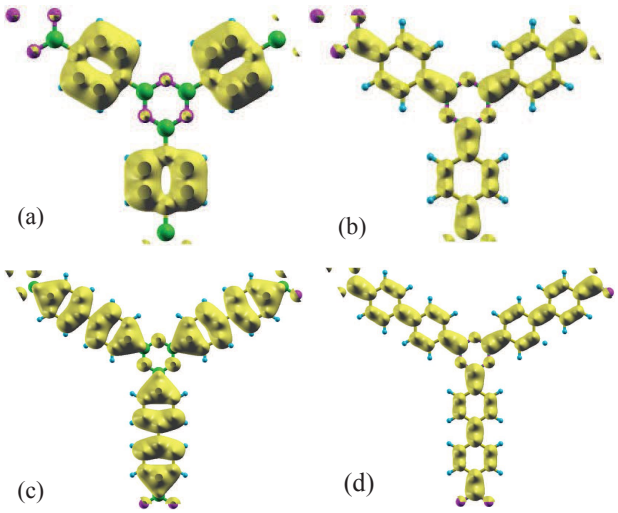

Fig. 5 (Color online). The local density of states are shown. For benzene-1, they are integrated between two given energies [-6.027, -6.010] eV (a) and [-2.520, -2.511] eV (b), respectively. For benzene-2, they are integrated between two given energies [-5.321, -5.250] eV (c) and [-2.460, -2.440] eV (d), respectively. The energy ranges which are chosen to calculate the local density of states are slightly larger than the shaded areas shown in Figs. 2(c, d) and 4(a, b).

ic properties, we further give the spatial distribution of the local density of states near the Fermi level. Figs. 5(a,b) show the local density of states for the frontier orbitals of benzene-1. They are integrated between two given energies [-6.027, -6.010] eV for HOMO and [-2.520, -2.511] eV for LUMO, respectively. Like graphene, the frontier orbitals mainly attribute to the delocalized $\pi-$conjugated electrons. However, the boroxine ring possesses little aromaticity and can not effectively serve as an electron-transferring bridge. Therefore, the conduction and valence bands near the Fermi level show the flat-band characteristics. According to the aromatical theory, LUMO's electron density is not identical to that of HOMO: the former partly localizes at the nodes while the latter is primarily distributed along the phenyl chains. Thus, the changes in chain lengths significantly affect the features of the ionization potential and only slightly alter the electronic affinity. For benzene-2, the local density of states are shown in Figs. 5(c, d) and the ranges of two given energies are [-5.321, -5.250] eV and [-2.460, -2.440] eV, respectively. The panel (c) is a representative 2-node system according to the aromatical theory. Two highest occupied bands of benzene-2 should localize in the same energy range as those of benzene-1 (Fig. 2(c)), but two C-C bonds along the benzene ring direction get shorten (Fig. 11) which makes two highest occupied bands split off. At last, the cyclic nature of benzene restricts against having an odd number of nodes. Thus, the valence bands are mainly

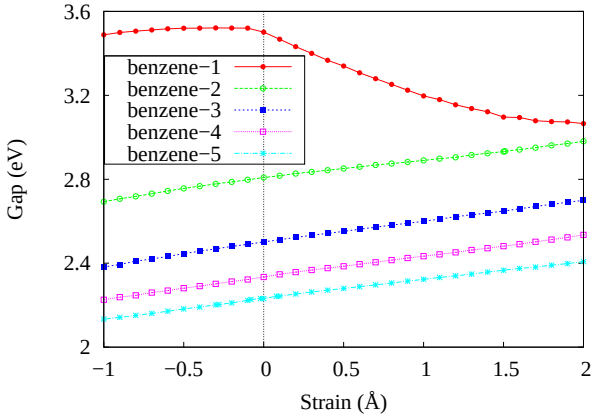

Fig. 6 (Color online). The band gaps of 2D boroxine-linked COFs (n=1, 2, 3, 4, and 5.) as a function of hydrostatic strains (ε).

the unfilled orbitals with 4 nodes, which is agreement with the local density of states shown in Figs. 5(b, d).

Inspired by the previous results of the strained 2D materials,[37,38] in the following section, we will discuss the variations of the electronic properties under hydrostatic strains in the range of [-1.0, 2.0] Å. The hydrostatic strains are imposed by scaling the lattice constants (a_n). $\varepsilon = (a - a_0)$, where a_0 and a are the equilibrium and stretched lattice constants, respectively. Under every strain, the COFs are fully relaxed (not only in-plane but also out-of-plane degrees of freedom) until the residual maximum forces are less than 0.01 eV/Å. And then, the electron properties for every equilibrium geometry are calculated and shown in Fig. 6. For all 2D boroxine-linked COFs, they are still semiconductors and their band gaps can be continuously modulated by the hydrostatic strains in the range of [-1.0, 2.0] Å. More interestingly, for benzene-1, the band gap continuously decreases, while it will monotonously increase for benzene-n (n $\geq$ 2) boroxine-linked COFs.

Specifically, there is an asymmetry adjustment of the band gap for benzene-1 under the hydrostatic strain. In other words, the band gap is robust under the compressive strain (the neg-

Table 2 The band gap, electronic affinity, and ionization potential in units of eV for 2D boroxine-linked COFs with a series of benzene rings of different length (n) under the compressive strain (ε^c = -1.0 Å) and the tensile strain (ε^t = 2.0 Å).

n	band gap		electronic affinity		ionization potential	
	-1.0	2.0	-1.0	2.0	-1.0	2.0
1	3.49	3.07	-2.33	-2.55	-5.82	-5.62
2	2.69	2.98	-2.34	-2.56	-5.03	-5.54
3	2.39	2.71	-2.32	-2.51	-4.71	-5.22
4	2.23	2.54	-2.31	-2.48	-4.54	-5.01
5	2.14	2.41	-2.31	-2.45	-4.45	-4.86

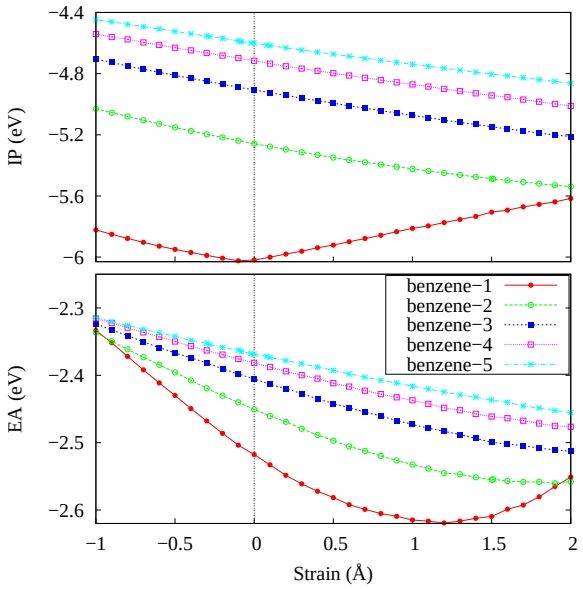

Fig. 7 (Color online). The energies of electronic affinity (EA, eV) and ionization potential (IP, eV) of a series of 2D boroxine-linked COFs as a function of hydrostatic strains (ε).

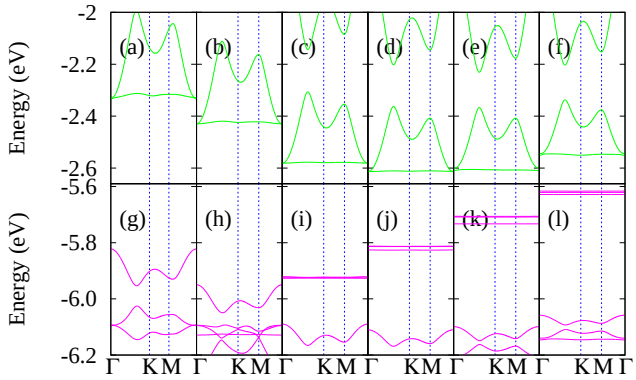

Fig. 8 (Color online). The band structures of 2D boroxine-linked COF with only one benzene ring connected between two boroxine rings under some given strains. Panels (a, g) are under -1.0 Å, (b, h) under -0.5 Å, (c, i) under 0.5 Å, (d, j) under 1.0 Å, (e, k) under 1.5 Å, and (f, l) under 2.0 Å.

ative value), while the tensile strain (the positive value) will make the band gap reduce to $\sim$ 3.07 eV under the tensile strain (ε^t = 2.0 Å), as shown in Table II. When the length of phenyl chains is equal or greater than 2, regardless of the compressive or tensile strains in the range of [-1.0, 2.0] Å, the band gaps will continuously and monotonously increase. For example, the band gap increases from 2.69 eV (ε^c = -1.0 Å) to 2.98 eV (ε^t = 2.0 Å) for benzene-2. No matter of the length of benzene rings, the increase of their band gaps is nearly linear as a function of ε and the accommodative amplitude of their band gaps is about 0.3 eV. Further, it is a worthy question to explore: how the valence and conduction bands shift with the strains. Fig. 7 shows the energies of the electronic affinity and ionization potential with respect to the hydrostatic strains. For 2D boroxine-linked COFs except for benzene-1, the electronic affinity and ionization potential will decrease at the same time whether the hydrostatic strain is compressive or tensile. For benzene-4, the ionization potential and electronic affinity monotonically decrease from -4.54 eV (ε^c = -1.0 Å) to -5.01 eV (ε^t = 2.0 Å) and from -2.31 eV (ε^c = -1.0 Å) to -2.48 eV (ε^t = 2.0 Å), respectively. In short, the increase of their band gaps can be mainly attributed to the drop of valence bands.

In comparison with all other COFs investigated in this manuscript, the electronic affinity and ionization potential of benzene-1 vary differently with the hydrostatic strain. Therefore, the band structures of benzene-1 under some given strains are shown in Fig. 8. From the upper panels, it is found that the LUMO's characteristics are the same. Still, for the electronic affinity, it firstly decreases and then increases with the strain in the range of [-1.0, 2.0] Å. This is because that their electron densities partly localize at the B-C bonds (B_0) which mainly contribute to the strains, as shown in Fig. 11. The other part of the LUMO's electron densities distributes around the C-C bonds (B_2) in the benzene rings. Moreover, these bonds linearly increase which further makes the electronic affinity decrease. On the other hand, the ionization potential increases with the tensile strain, which directly induces the band gap to drop. From the down panels of Fig. 8, the valence bands have different features under different types of strains. So, the local density of states of HOMO for strained benzene-1 are calculated and shown in Fig. 9. In comparison with the local density of states, the HOMO's electron densities show zero nodes under the compressive strain while they show 2 nodes under the tensile strain. Therefore, HOMO is dependent on the C-C bonds under the compressive strain, while it is dependent on the A_1 angle under the tensile strain. Furthermore, HOMO will shift to the Fermi level with the enhancement of π-electrons induced by the bond length decreasing as well as the A_1 angle increasing.

In order to discuss their mechanical properties, the Young's

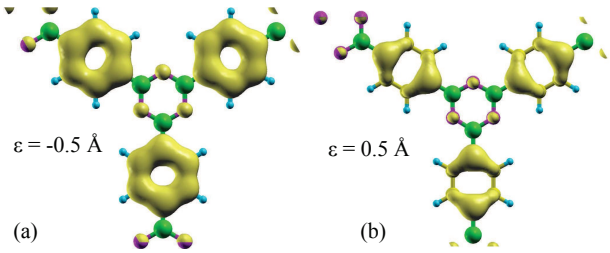

Fig. 9 (Color online). The local density of states for the strained benzene-1 are shown. (a) For ε^c = -0.5 Å, it is integrated between the given energies [-6.086 -5.886] eV. (b) For ε^t = 0.5 Å, it is integrated between the given energies [-6.166, -6.066] eV.

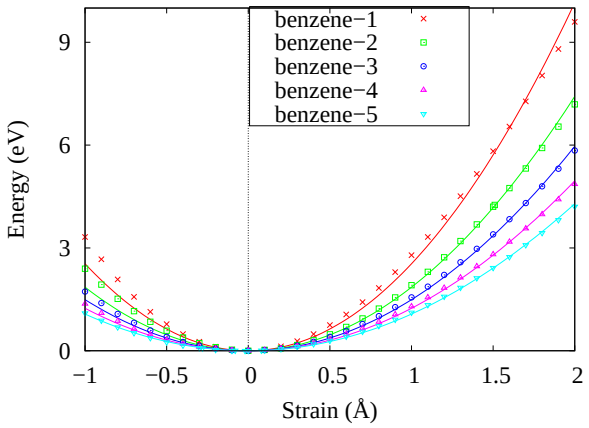

Fig. 10 (Color online). Schematic illustration of the strain energies as a function of strains (ε). The data are self-consistently calculated points and the lines are fitted with the least-square method.

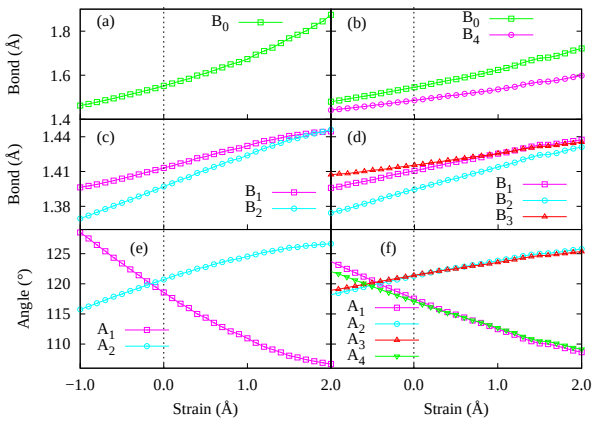

Fig. 11 (Color online). Schematic illustration of the bond lengths and bond angles as a function of strains (ε). All the bonds and angles are marked in Fig. 1. Panels (a, c, e) and (b, d, f) refer to the benzene-1 and benzene-2, respectively.

modulus[39] are calculated *via* the equation $Y^{2D} = \partial^2 E_s/\partial\varepsilon^2$. Since their total energies account for their lattice constants (a_n), the strain energies (E_s) can be expressed as a function of only the macroscopic deformation gradient (ε), i.e., $E_s = E(\varepsilon) = E(a) - E(a_0)$, namely, the total energies at a given hydrostatic strain (ε) minus those at zero strain. The strain energies as a function of hydrostatic strains are shown in Fig. 10. The variation of the total energies with the hydrostatic strains show a nearly parabolic behavior and do not exhibit discontinuous changes in the range of [-1.0, 2.0] Å. That is to say, 2D boroxine-linked COFs sustain original atomic configurations and mechanical stabilities. Obviously, 2D boroxine-linked COFs could keep stable in a more large strain range than graphene and γ-graphyne,[40–43] especially under the compressive strains which induce the wrinkling instabilities (see Supporting Information Fig. S10).

Like graphene, the thickness of a monolayer boroxine-linked COF could be assumed as 0.34 nm. The Young's modulus are obtained by using the least-squares method and shown in Table. III, which are 40.70, 30.76, 24.03, 19.71, and 16.82 N m^{-1} for benzene-1, -2, -3, -4, and -5 boroxine-linked COFs, respectively. It is found that 2D boroxine-linked COFs become softer and softer with increasing the length of phenyl rings due to the weaker C-C bonds (B_4, Fig. 11(b)) between phenyl rings. In comparison with graphene, the Young's modulus of 2D boroxine-linked COFs are one order smaller than that of graphene (340 N m^{-1}). This can be attributed to the porous properties and the weaker C-B bonds (B_0, Fig. 11(a, b)) connected between the boroxine and benzene rings.[44,45] Compared boroxine-linked COFs with γ-graphyne, although both of them are the porous structure, 2D boroxine-linked COFs are much softer and the Young's modulus are just one fifth of that of γ-graphyne sheet ($\sim$ 162 N m^{-1})[46] due to a combination of boroxine ring strain and the lability of the B-O bonds.[47]

Table 3 The fitted parameters ($E_\varepsilon = a\times\varepsilon^2 + b\times\varepsilon + c$) are calculated by using the least-squares method.

	a (eV/Å^2)	b (eV/Å)	c (eV)
benzene-1	2.54 ± 0.05	-0.17 ± 0.07	0.20 ± 0.05
benzene-2	1.92 ± 0.02	-0.18 ± 0.03	0.09 ± 0.02
benzene-3	1.50 ± 0.01	-0.05 ± 0.02	0.05 ± 0.01
benzene-4	1.23 ± 0.01	-0.02 ± 0.01	0.04 ± 0.01
benzene-5	1.05 ± 0.01	+0.02 ± 0.01	0.02 ± 0.01

4 Conclusions

The electronic properties and Young's modulus of a new kind of two-dimensional materials, boroxine-linked covalent organic frameworks, are studied under the uniform compressive/tensile strains within density functional theory. Owing to the π-conjugated electrons around the phenyl rings, the systems show flat bands in the vicinity of Fermi level. Their band gaps can be tuned by increasing the phenyl chain and are basically saturated when the length of benzene ring is 9. We demonstrate that, for benzene-1 boroxine-linked COFs, the band gap exhibits an asymmetry in tensile versus compressive strains which implicates that strain engineering of its devices is only viable with the application of tensile strain but difficult with the compressive strain. When n $\geq$ 2, all of them are semiconductors with the controllable band gaps, depending on the phenyl chain and the applied strain. Furthermore, their band gaps increase steadily and monotonously with increasing the strain in the range of [-1.0, 2.0] Å. Therefore, the electronic

properties can be readily engineered by applying moderate strains. In addition, the torsion of phenyl rings plays an important role in the electronic properties of benzene-n boroxine-linked COFs when n $>$ 3 (see Supporting Information Figs. S3, S5, S7 and S9), but it is very complex - especially when n is even. At last, boroxine-linked COFs are much softer than graphene as well as γ-graphyne and more stable in a larger strain range.

5 ACKNOWLEDGEMENT

This work was supported by the National Natural Science Foundation of China under Grant No. 51372064 and the Natural Science Foundation of Hebei Province (No. 2013201249 and No. A2014201176). The calculations were supported by the High-Performance Computing Center of Hebei University.

References

1 K. S. Kim, Y. Zhao, H. Jang, S. Y. Lee, J. M. Kim, K. S. Kim, J.-H. Ahn, P. Kim, J.-Y. Choi and B. H. Hong, *Nature*, 2009, **457**, 706.
2 A. Lipp, K. A. Schwetz and K. Hunold, *Journal of the European Ceramic Society*, 1988, **5**, 3.
3 L. F. Mattheiss, *Phys. Rev. B*, 1973, **8**, 3719.
4 P. Vogt, P. D. Padova, C. Quaresima, J. Avila, E. Frantzeskakis, M. C. Asensio, A. Resta, B. Ealet and G. L. Lay, *Phys. Rev. Lett.*, 2012, **108**, 155501.
5 L. Li, S. zan Lu, J. Pan, Z. Qin, Y. qi Wang, Y. Wang, C. yu Cao, S. Du and H.-J. Gao, *Adv. Mater.*, 2014, **26**, 4820.
6 D. Warschauer, *J. Appl. Phys.*, 1963, **34**, 1853.
7 L. Li, Y. Wang, S. Xie, X.-B. Li, Y.-Q. Wang, R. Wu, H. Sun, S. Zhang and H.-J. Gao, *Nano Lett.*, 2013, **13**, 4671.
8 D. Akinwande, N. Petrone and J. Hone, *Nature Commun.*, 2014, **5**, 5678.
9 T. Roy, M. Tosun, J. S. Kang, A. B. Sachid, S. B. Desai, M. Hettick, C. C. Hu and A. Javey, *ACS Nano*, 2014, **8**, 6259.
10 A. P. Côté, A. I. Benin, N. W. Ockwig, M. O'Keeffe, A. J. Matzger and O. M. Yaghi, *Science*, 2005, **310**, 1166.
11 D. F. Perepichka and F. Rosei, *Science*, 2009, **323**, 216.
12 A. Nagai, Z. Guo, X. Feng, S. Jin, X. Chen, X. Ding and D. Jiang, *Nature Commun.*, 2011, **2**, 536.
13 S. S. Han, H. Furukawa, O. M. Yaghi and W. A. Goddard, *J. Am. Chem. Soc.*, 2008, **130**, 11580.
14 J. L. Mendoza-Cortés, S. S. Han and W. A. Goddard, *J. Phys. Chem. A*, 2012, **116**, 1621.
15 G. H. V. Bertrand, V. K. Michaelis, T.-C. Ong, R. G. Griffin and M. Dinca, *Proc. Natl. Acad. Sci. USA*, 2013, **110**, 4923.
16 X. Feng, L. Liu, Y. Honsho, A. Saeki, S. Seki, S. Irle, Y. Dong, A. Nagai and D. Jiang, *Angew. Chem.*, 2012, **124**, 2672.
17 M. Calik, F. Auras, L. M. Salonen, K. Bader, I. Grill, M. Handloser, D. D. Medina, M. Dogru, F. Löbermann, D. Trauner, A. Hartschuh and T. Bein, *J. Am. Chem. Soc.*, 2014, **136**, 17802.
18 C.-Z. Guan, D. Wang and L.-J. Wan, *Chem. Commun.*, 2012, **48**, 2943.
19 J. F. Dienstmaier, D. D. Medina, M. Dogru, P. Knochel, T. Bein, W. M. Heckl and M. Lackinger, *ACS Nano*, 2012, **6**, 7234.
20 E. L. Spitler and W. R. Dichtel, *Nature Chem.*, 2010, **2**, 672.
21 S. Clair, M. Abel and L. Porte, *Chem. Commun.*, 2014, **50**, 9627.
22 P. Zhu and V. Meunier, *J. Chem. Phys.*, 2012, **137**, 244703.
23 S.-L. Cai, Y.-B. Zhang, A. B. Pun, B. He, J. Yang, F. M. Toma, I. D. Sharp, O. M. Yaghi, J. Fan, S.-R. Zheng, W.-G. Zhang and Y. Liu, *Chem. Sci.*, 2014, **5**, 4693.
24 S.-M. Choi, S.-H. Jhi and Y.-W. Son, *Phys. Rev. B*, 2010, **81**, 081407(R).
25 H. Rostami and R. Asgari, *Phys. Rev. B*, 2012, **86**, 155435.
26 W. Kohn and L. J. Sham, *Phys. Rev*, 1965, **140**, A1133.
27 J. M. Soler, E. Artacho, J. Gale, D. A. Garacia, J. Junquera, P. Ordejon and D. Sanchez-Portal, *J. Phys.: Condens. Matter*, 2002, **14**, 2745.
28 J. P. Perdew, K. Burke and M. Ernzerhof, *Phys. Rev. Lett.*, 1996, **77**, 3865.
29 D. R. Hamann, M. Schlüter and C. Chiang, *Phys. Rev. Lett.*, 1979, **43**, 1494.
30 H. J. Monkhorst and J. D. Pack, *Phys. Rev. B*, 1976, **13**, 5188.
31 R. Al-Jishi and G. Dresselhaus, *Phys. Rev. B*, 1982, **26**, 4514.
32 T. Faury, S. Clair, M. Abel, F. Dumur, D. Gigmes and L. Porte, *J. Phys. Chem. C*, 2012, **116**, 4819.
33 L. Türker, S. Gümüş and T. Atalar, *Bull. Korean Chem. Soc*, 2009, **30**, 2233.
34 P. W. Fowler and E. Steiner, *J. Phys. Chem. A*, 1997, **101**, 1409.
35 P. von Ragué Schleyer, H. Jiao, N. J. R. van Eikema Hommes, V. G. Malkin and O. L. Malkina, *J. Am. Chem. Soc.*, 1997, **119**, 12669.
36 W. Wu, W. Guo and X. C. Zeng, *Nanoscale*, 2013, **5**, 9264.
37 P. L. de Andres, F. Guinea and M. I. Katsnelson, *Phys. Rev. B*, 2012, **86**, 245409.
38 M. Topsakal, S. Cahangirov and S. Ciraci, *Appl. Phys. Lett.*, 2010, **96**, 091912.
39 H. Zhao, K. Min and N. R. Aluru, *Nano Lett.*, 2009, **9**, 3012.
40 S. Bae, H. Kim, Y. Lee, X. Xu, J.-S. Park, Y. Zheng, J. Balakrishnan, T. Lei, H. R. Kim, Y. I. Song, Y.-J. Kim, K. S. Kim, B. Özyilmaz, J.-H. Ahn, B. H. Hong and S. Iijima, *Nature Nanotech.*, 2010, **5**, 574.
41 C. Lee, X. Wei, J. W. Kysar and J. Hone, *Science*, 2008, **321**, 385.
42 Y. Zhang and F. Liu, *Appl. Phys. Lett.*, 2011, **99**, 241908.
43 R.-N. Wang, X.-H. Zheng, H. Hao and Z. Zeng, *J. Phys. Chem. C*, 2014, **118**, 23328.
44 N. Mounet and N. Marzari, *Phys. Rev. B*, 2005, **71**, 205214.
45 K. V. Zakharchenko, M. I. Katsnelson and A. Fasolino, *Phys. Rev. Lett.*, 2009, **102**, 046808.
46 Q. Peng, W. Ji and S. De, *Phys. Chem. Chem. Phys.*, 2012, **14**, 13385.
47 J. Beckmann, D. Dakternieks, A. Duthie, A. E. K. Lim and E. R. T. Tiekink, *Journal of Organometallic Chemistry*, 2001, **633**, 149.

Table 1 The lattice constants (a_n,Å), bond lengths (Å), angles (°), and dihedral angles (°) of the free-standing 2D boroxine-linked COFs as a function of the phenyl lengths (n).

n	a_n	O-B	B-C	C-C[1]	C-C[2]	∠BOB	∠OBO	∠C-CC-C[3]	∠C-CB-O[4]
1	15.11	1.38	1.55	1.41	1.41	121.06	118.92	—	1.73
2	22.66	1.38	1.55	1.39	1.42	120.90	119.15	0.17	0.35
3	30.26	1.38	1.55	1.38	1.42	121.01	119.01	0.10	0.28
4	37.84	1.38	1.55	1.39	1.41	121.05	119.00	0.00	0.05
5	45.42	1.38	1.54	1.39	1.41	120.95	118.95	0.04	0.24

[1] Two carbon-carbon bond lengths in the benzene rings along the direction of benzene rings.
[2] The other four carbon-carbon bond lengths in the benzene rings except two carbon-carbon bonds along the direction of benzene rings.
[3] The dihedral angle between two benzene rings.
[4] The dihedral angle between the benzene ring and boroxine ring.